

Plasmoid-induced-reconnection and fractal reconnection

Kazunari Shibata¹ and Syuniti Tanuma²

¹Kwasan Observatory, Kyoto University, Yamashina, Kyoto 607-8471, Japan

²STE Laboratory, Nagoya University, Toyokawa, Aichi 442-8507, Japan

(Received June 28, 2000; Revised November 10, 2000; Accepted February 28, 2001)

As a key to understanding the basic mechanism for fast reconnection in solar flares, *plasmoid-induced-reconnection* and *fractal reconnection* are proposed and examined. We first briefly summarize recent solar observations that give us hints on the role of plasmoid (flux rope) ejections in flare energy release. We then discuss the plasmoid-induced-reconnection model, which is an extension of the classical two-ribbon-flare model which we refer to as the CSHKP model. An essential ingredient of the new model is the formation and ejection of a plasmoid which play an essential role in the storage of magnetic energy (by inhibiting reconnection) and the induction of a strong inflow into reconnection region. Using a simple analytical model, we show that the plasmoid ejection and acceleration are closely coupled with the reconnection process, leading to a *nonlinear instability* for the whole dynamics that determines the macroscopic reconnection rate uniquely. Next we show that the current sheet tends to have a *fractal structure* via the following process path: tearing \Rightarrow sheet thinning \Rightarrow Sweet-Parker sheet \Rightarrow secondary tearing \Rightarrow further sheet thinning $\Rightarrow \dots$. These processes occur repeatedly at smaller scales until a microscopic plasma scale (either the ion Larmor radius or the ion inertial length) is reached where anomalous resistivity or collisionless reconnection can occur. The current sheet eventually has a fractal structure with many plasmoids (magnetic islands) of different sizes. When these plasmoids are ejected out of the current sheets, fast reconnection occurs at various different scales in a highly time dependent manner. Finally, a scenario is presented for fast reconnection in the solar corona on the basis of above *plasmoid-induced-reconnection in a fractal current sheet*.

1. Introduction

Recent numerical simulations (e.g., Ugai, 1986, 1992; Scholer, 1989; Biskamp, 1986; Yan *et al.*, 1992; Yokoyama and Shibata, 1994; Magara and Shibata, 1999; Tanuma *et al.*, 1999, 2001) have revealed that if the resistivity is spatially uniform, fast, steady-state Petscheck-type reconnection does not occur but instead slow, Sweet-Parker-type reconnection occurs. This holds especially when a strong inflow is imposed at the external boundary, and the only way so far found to achieve a steady-state Petscheck configuration is to have a *localized resistivity*. The so called anomalous resistivity satisfies this condition. However, there are a number of questions about it.

1. In order to produce anomalous resistivity, the current sheet thickness must be as small as the ion Larmor radius¹

$$r_{L,ion} = \frac{m_i v_{th} c}{e B} = 100 \left(\frac{B}{10 \text{ G}} \right)^{-1} \left(\frac{T}{10^6 \text{ K}} \right)^{1/2} \text{ cm} \quad (1)$$

or the ion inertial length

$$l_{in,ion} = c/\omega_{p,i} = 300 \left(\frac{n}{10^{10} \text{ cm}^{-3}} \right)^{-1/2} \text{ cm}, \quad (2)$$

¹Although the physics of anomalous resistivity has not yet been fully understood, it is known that anomalous resistivity occurs due to plasma turbulence which is produced by the microscopic plasma instability, such as the lower hybrid drift instability, the electrostatic ion cyclotron instability,

both of which are of order of 1 m in the solar corona. Since the size of solar flares is typically 10⁴ km, there is a large gap between the flare size and the necessary microscopic scale to produce anomalous resistivity. How can such an enormous gap between macroscopic and microscopic scales be reconciled in real flares?

2. Even if the anomalous resistivity (or localized resistivity) is realized, what determines the reconnection rate?

Based on recent observations of solar flares and numerical simulations, we try to give possible answers to above questions. We argue that the key physics needed to answer the above questions is the global coupling between plasmoid (flux rope) ejection and reconnection process. Since this coupling is scale free, it can occur on any scale, constituting a fractal reconnection process, which couples the macro- and micro-scales.

2. Solar Observations: Flares and Plasmoid Ejections

Yohkoh has revealed numerous indications of magnetic reconnection in solar flares, such as cusps, arcades, loop top hard X-ray (HXR) sources, X-ray jets, and so on (e.g., Tsuneta *et al.*, 1992a; Hanaoka *et al.*, 1994; Masuda *et al.*,

and the ion sound instability (e.g., Treumann and Baumjohann, 1997). In the case of the lower hybrid drift instability, the threshold of the instability is $v_d > v_{ion,th}$ where $v_d = j/(ne)$ is the electron-ion drift velocity, and $v_{ion,th} = (kT/m_i)^{1/2}$ is the ion thermal speed. This equation becomes equivalent to $d < r_{L,ion}$ if we consider the pressure balance $p = 2nkT \simeq B^2/8\pi$ between inside and outside of the current sheet, where d is the thickness of the current sheet.

1994; Forbes and Acton, 1996; Shibata, 1999). Furthermore, as has been predicted by some pioneers (Hirayama, 1991; Moore and Roumeliotis, 1992), the association of plasmoid (flux rope) ejections with flares is much more common than had been thought (e.g., Shibata *et al.*, 1995; Nitta, 1996; Ohya and Shibata, 1997, 1998, 2000; Tsuneta, 1997; Akiyama and Hara, 2000). This has led us to advocate a unified model of flares shown in Fig. 1 (Shibata *et al.*, 1995; Shibata, 1996, 1997, 1998, 1999). Recent observations with SOHO/LASCO have also revealed a lot of evidence of flux rope and disconnection events in coronal mass ejections (CMEs) (e.g., Dere *et al.*, 1999; Simnet *et al.*, 1997), and Yokoh has shown that giant arcades formed after prominence eruptions or CMEs are physically similar to flare arcades even though their total X-ray intensity is much lower than that of normal flares (e.g., Tsuneta *et al.*, 1992b; Hanaoka *et al.*, 1994). Figure 2 shows several examples of plasmoid (flux rope) ejections on the Sun from the largest scale in CMEs ($\sim 10^{11}$ cm) to the smallest scale in compact flares ($\sim 10^9$ cm). The velocity of these plasmoids range from a few 10 km/s to 1000 km/s, and their maximum values are comparable to the inferred coronal Alfvén speed (~ 1000 km/s). These images show that the magnetic reconnection and associated plasmoid ejection universally occur on widely different scales.

One of the interesting findings by Yokoh concerning X-ray plasmoid ejections is that, in impulsive flares, a plasmoid starts to be ejected slowly, long before the impulsive

phase, and then is rapidly accelerated during the impulsive phase (Ohya and Shibata, 1997, 1998; Tsuneta, 1997; Fig. 3). Similar behavior has also been observed for LDE flares and CME events (e.g., Kahler *et al.*, 1988; Hundhausen, 1999).

Another interesting finding from Yokoh on X-ray plasmoid ejection is that *there is a positive correlation between the plasmoid velocity ($V_{plasmoid} \sim 30\text{--}400$ km/s) and the apparent rise velocity of the flare loop ($V_{loop} \sim 4\text{--}20$ km/s)* (Shibata *et al.*, 1995):

$$V_{plasmoid} \simeq (8 - 20) \times V_{loop}. \quad (3)$$

This relation (though still very preliminary) suggests that the plasmoid velocity is related to the reconnection inflow speed, or vice-versa. This is because the apparent rise motion of the flare loop is coupled to the reconnection process. Consequently, magnetic flux conservation leads to

$$V_{loop} \simeq (B_{inflow}/B_{loop})V_{inflow}. \quad (4)$$

Morimoto and Kurokawa (2000) found a correlation between the erupting velocity of H-alpha filaments (i.e., a plasmoid) and the thermal energy density of post-eruption X-ray arcades. This also suggests that there is a physical relation between plasmoid velocity and inflow speed (reconnection rate).

3. Role of Plasmoid: Plasmoid-Induced-Reconnection Model

On the basis of these observations, Shibata (1996, 1997) proposed a *plasmoid-induced-reconnection model*, which is an extension of the classical CSHKP (Carmichael, 1964; Sturrock, 1966; Hirayama, 1974; Kopp and Pneuman, 1976) model and similar in spirit to the model of Anzer and Pneuman (1982). In this model, the plasmoid ejection plays a key role in triggering fast reconnection in two different ways (Fig. 1).

1) *A plasmoid (flux rope) can store energy by inhibiting reconnection.* A large magnetic island (plasmoid or flux rope) inside the current sheet is a big obstacle for reconnection. Hence if an external force compresses the current sheet, magnetic energy can be stored around the current sheet. Only after the plasmoid is ejected out of the current sheet, will the anti-parallel field lines be able to touch and reconnect. If a larger plasmoid is ejected, a larger energy release occurs.

2) *A plasmoid ejection can induce a strong inflow into the reconnection site.* If a plasmoid is suddenly ejected out of the current sheet at the velocity $V_{plasmoid}$, an inflow must develop toward the X-point in order to compensate for the mass ejected by the plasmoid, as has been shown in many numerical simulations (e.g., Forbes, 1990; Yokoyama and Shibata, 1994, 2001; Magara *et al.*, 1997; Tanuma *et al.*, 2001; see also Fig. 4). The inflow speed can be estimated from the mass conservation law (assuming incompressibility, for simplicity);

$$V_{inflow} \sim V_{plasmoid} W_{plasmoid} / L_{inflow}, \quad (5)$$

where $W_{plasmoid}$ is the typical width of the plasmoid, and $L_{inflow} (\geq W_{plasmoid})$ is the typical vertical length of the inflow region. In deriving Eq. (5), it is assumed that the

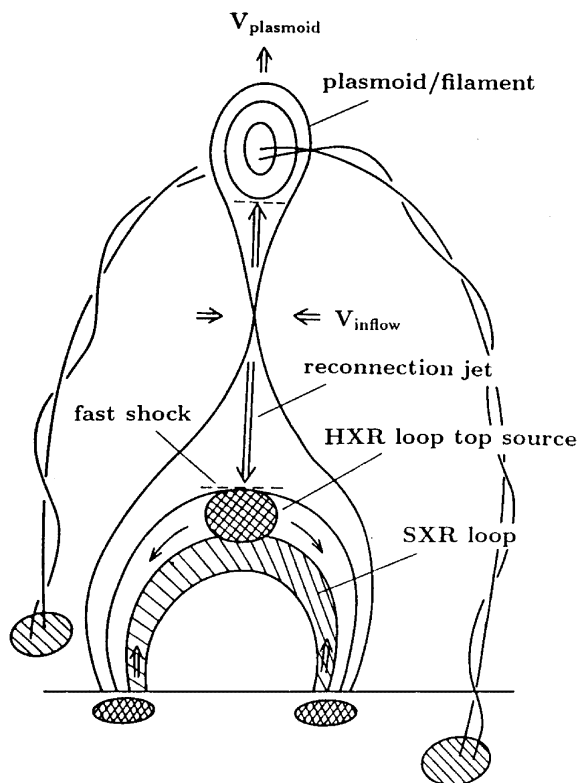


Fig. 1. A unified model of flares: *plasmoid-induced-reconnection model* (Shibata *et al.*, 1995). This is an extension of a classical model of eruptive solar flares, called the CSHKP model.

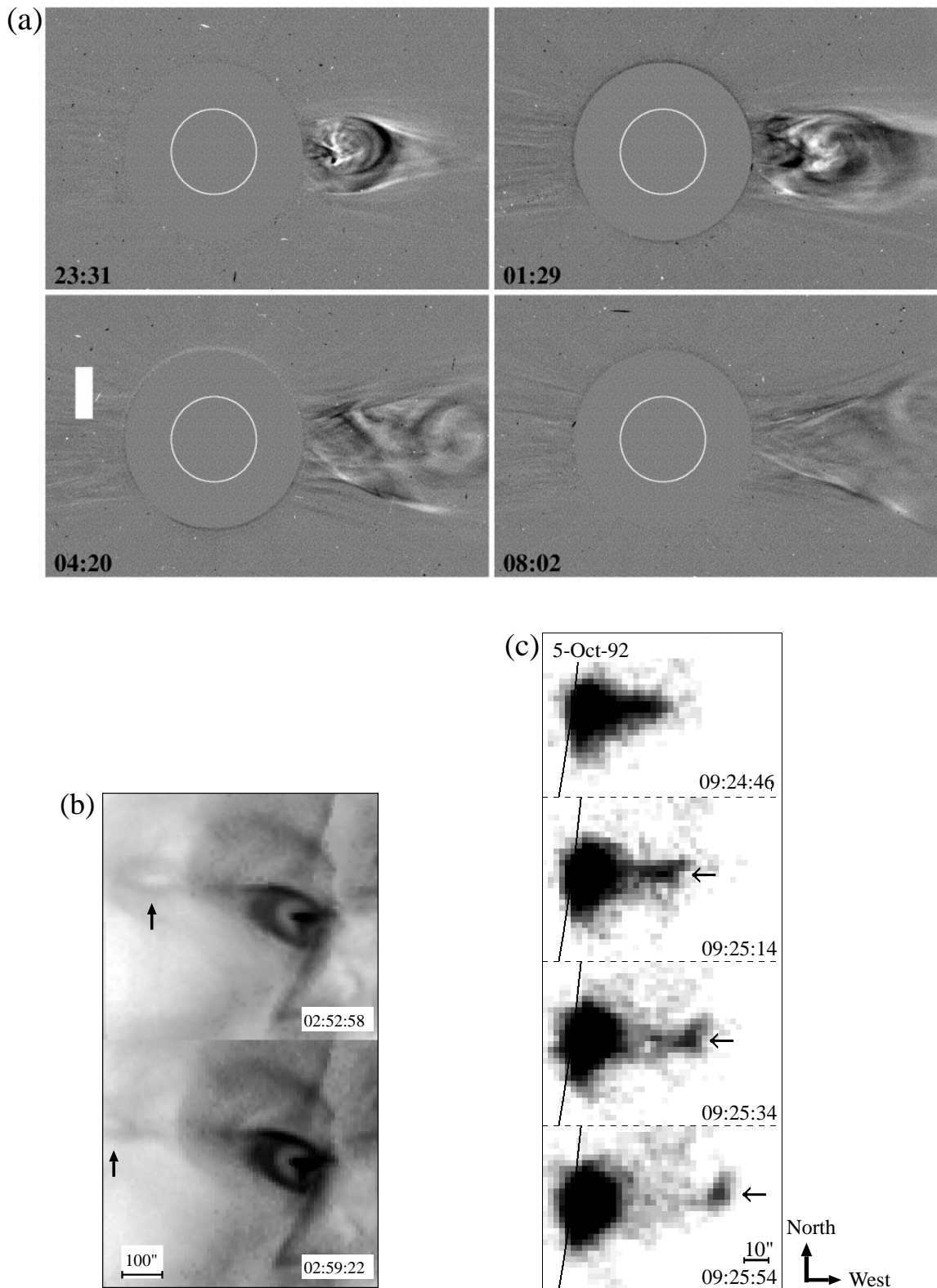


Fig. 2. Various plasmoids (flux rope) with different scales observed on the Sun. (a) Coronal mass ejection (CME), the largest-scale plasmoid on the Sun ($\sim 10^{11}$ cm) observed with SOHO/LASCO on Nov. 1–2, 1997 (Dere *et al.*, 1999). These are running-difference images. The velocity of the CME is 140–240 km/s. (b) Large-scale X-ray plasmoid associated with an LDE (long duration event) flare on Feb. 21, 1992 ($\sim 10^{10}$ cm) observed with Yohkoh/SXT (Hudson, 1994; Ohya and Shibata, 1998). The plasmoid velocity is about 100 km/s. (c) Small-scale X-ray plasmoid associated with an impulsive flare ($\sim 10^9$ cm) observed with Yohkoh/SXT on Oct. 5, 1992 (Ohya and Shibata, 1998). These are negative images. The velocity of the plasmoid is 250–500 km/s. 1" corresponds to 726 km.

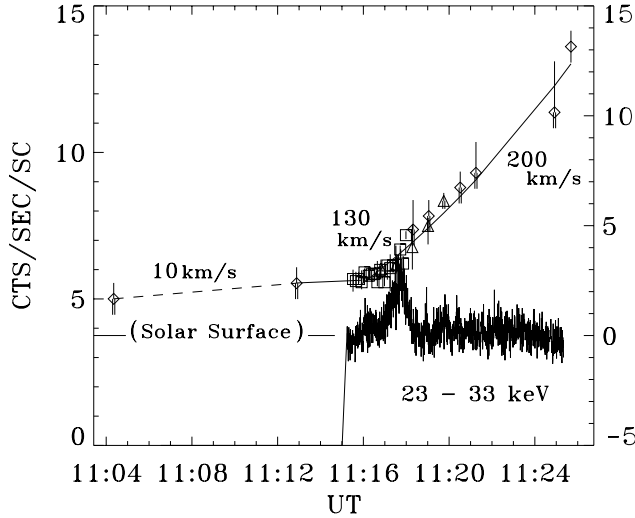


Fig. 3. Temporal variations of the height of an X-ray plasmoid and the hard X-ray intensity of an impulsive solar flare on 11 Nov. 1993 observed with Yohkoh SXT and HXT (Ohyama and Shibata, 1997).

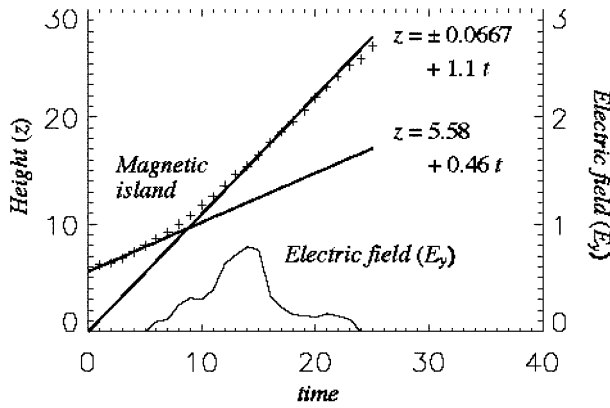


Fig. 4. Temporal variations of both the reconnection rate (electric field at the reconnection-point) and the height of the plasmoid (magnetic island) for a typical result of 2.5D MHD numerical simulation of magnetic reconnection induced by plasmoid (flux rope) ejection (Magara *et al.*, 1997). Units of the height, time, and electric field are L (a half length between footpoints of a sheared arcade loop), $t_0 = L/C_{s0}$ (C_{s0} is the sound speed $\sim 0.4V_A$), and $E_0 = C_{s0}B_0/c$, respectively. In a typical solar coronal condition, $L \simeq 5000$ km, $V_A \simeq 1000$ km/s, $E_0 \simeq 2 \times 10^4$ V/m, and $t_0 \simeq 20$ sec.

mass flux into reconnection region ($\sim L_{inflow} V_{inflow}$) is balanced by the mass flux carried by the plasmoid motion ($\sim V_{plasmoid} W_{plasmoid}$). Since the reconnection rate is determined by the inflow speed, the ultimate origin of fast reconnection in this model is the fast ejection of the plasmoid. If the plasmoid ejection (or outflow) is inhibited in some way, then fast reconnection ceases (Ugai, 1982; Tanuma *et al.*, 2001; Lin and Forbes, 2000).

This model naturally explains (1) the strong acceleration of plasmoids during the impulsive (rise) phase of flares (see Fig. 3 and next section), (2) the positive correlation between plasmoid velocity and the apparent rise velocity of flare loops (Eqs. (3) and (5)), (3) the total energy release rate of flares and plasmoid ejections (Shibata, 1997), and (4) the

time scale of the impulsive (rise) phase for both impulsive flares ($\sim L_{inflow}/V_{plasmoid} \sim 10^4$ km/100 km/s ~ 100 sec), and for LDE flares ($\sim 10^5$ km/100 km/s $\sim 10^3$ sec).

It is interesting to note that similar impulsive reconnection associated with plasmoid ejection (current sheet ejection) has also been observed in laboratory experiments (Ono *et al.*, 2001).

4. Nonlinear Instability Caused by Strong Coupling between Plasmoid Ejection (Acceleration) and Reconnection

In this section, we examine the physical mechanism of the *plasmoid-induced-reconnection* in more detail. We consider a situation where reconnection has just begun and a plasmoid, with a length L_p and a width W_p , has just started to form. The reconnection generates a jet (with the Alfvén speed V_A) which collides with the plasmoid and accelerates it. Thus the plasmoid speed increases with time, which induces a faster inflow into the reconnection point (i.e., the X-point), thereby leading to yet faster reconnection and an even larger energy release rate. This, in turn, accelerates the plasmoid again, eventually leading to a kind of nonlinear instability for the plasmoid ejection and the associated reconnection.

Let us estimate the plasmoid velocity in this process, by assuming that the plasmoid is accelerated solely by the momentum of the reconnection jet. (Note that we do not deny the possibility of acceleration of plasmoid by other mechanism such as global magnetic pressure. The purpose of this section is simply to show how the momentum of the reconnection jet can accelerate the plasmoid.) We also assume that the plasmoid density ρ_p and the ambient plasma density ρ are constant with time, for simplicity. In absence of any appropriate time-dependent theory in a rapidly evolving configuration, we assume that the steady state mass conservation $V_i L_i = V_p W_p$ (Eq. (5)) is valid and also that all the mass flux ($V_i L_i$) convected into the reconnection region (with length of L_i) are accelerated up to Alfvén speed as in Sweet-Parker or Petschek model.

We first consider the case in which the mass added to the plasmoid by the reconnection jet is much smaller than the total mass of the plasmoid (i.e., the plasmoid speed V_p is much smaller than the Alfvén speed V_A). Equating the momentum added by the reconnection jet with the change of momentum of the plasmoid, we have

$$\rho_p L_p W_p \frac{dV_p}{dt} = \rho V_i L_i V_A = \rho V_p W_p V_A \quad (6)$$

where we use the mass conservation relation for the inflow and the outflow, $V_p W_p = V_i L_i$ (Eq. 5). (See Appendix for detailed derivation of the Eq. (6).) Physically, this means that the inflow is induced by the outflow (plasmoid ejection). This is the reason why this reconnection is called *plasmoid-induced-reconnection*.

The equation (6) is easily solved to yield the solution

$$V_p = V_0 \exp(\omega t) \quad (7)$$

where V_0 is the initial velocity of the plasmoid, and

$$\omega = \frac{\rho V_A}{\rho_p L_p}. \quad (8)$$

Thus, the plasmoid velocity increases exponentially with time, and the “growth time” ($1/\omega$) is basically of order of Alfvén time. The inflow speed becomes

$$V_i = \frac{W_p}{L_i} V_p = \frac{W_p V_0 \exp(\omega t)}{L_i(0) + \frac{V_0}{\omega} (\exp(\omega t) - 1)}. \quad (9)$$

If W_p is constant, the inflow speed increases exponentially with time in the initial phase, but tends to be a constant ($\simeq \omega W_p$) in the late phase.

As time goes on, the mass added to the plasmoid by the jet increases and eventually becomes non-negligible compared with the initial mass (i.e., the plasmoid speed becomes non-negligible compared with the Alfvén speed). In this case, we obtain the solution (see Appendix for derivation):

$$V_p = \frac{V_A \exp(\omega t)}{\exp(\omega t) - 1 + V_A/V_0}. \quad (10)$$

Hence the plasmoid speed is saturated at around $t = t_c \simeq \frac{1}{\omega} \ln(V_A/V_0)$ and hereafter tends to the Alfvén speed V_A as time goes on. The inflow speed becomes

$$\begin{aligned} V_i &= \frac{W_p V_p}{L_i} \\ &= W_p \frac{V_A \exp(\omega t) / (\exp(\omega t) + a)}{(V_A/\omega) \ln[(\exp(\omega t) + a)/(1 + a)] + L_i(0)} \end{aligned} \quad (11)$$

where $a = V_A/V_0 - 1$. If W_p is constant in time, the inflow speed gradually decreases in proportion to $1/t$ after t_c .² On the other hand, if W_p increases with time in proportion to t after t_c , the inflow speed becomes constant,

$$V_i = \omega W_p(t=0) = \frac{\rho V_A}{\rho_p L_p} W_p(t=0). \quad (12)$$

In this case, the reconnection becomes steady, and the shape of the reconnection jet and plasmoid becomes self-similar in time and space (e.g., Nitta *et al.*, 2001; Yokoyama and Shibata, 2001).

A typical solution for $W_p = \text{constant}$ is shown in Fig. 5, which reminds us of the observed relation between plasmoid height vs. hard X-ray intensity (Fig. 3; Ohya and Shibata, 1997) and explains also the numerical simulation results (Fig. 4; Magara *et al.*, 1997) very well. It is noted here that the hard X-ray intensity is a measure of either the electric field at the reconnection point ($E \propto V_i B$) or the energy release rate ($\propto \text{Poynting flux} \propto V_i B^2 / (4\pi)$).

5. Fractal Reconnection

As we discussed in Section 1, we have a fundamental question: how can we reach the small dissipation scale necessary for anomalous resistivity or collisionless reconnection in solar flares? Also, even if we can reach such a small scale, is it true that there is only one diffusion region with a thickness of 100 cm (and with a length of 10 m or 100 m) in a solar flare as expected from Petschek’s steady state theory?

The idea that the reconnection process is inherently turbulent, involving a spectrum of different scales, has been

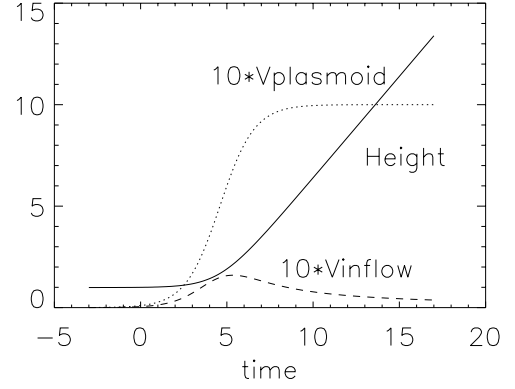


Fig. 5. Temporal variations of the plasmoid velocity ($V_{plasmoid}$), its height, and inflow velocity (V_{inflow}), in an analytical model (Eqs. (10) and (11)) for the case of $V_A/V_0 = 100$. Units of the velocity, height, and time are V_A , L_p , and L_p/V_A , respectively.

around for some time (see Ichimaru, 1975, for examples). However, here we argue that a plasma with large magnetic Reynolds number (occurs as in the solar corona, the interstellar medium, or the intergalactic medium) inevitably leads to a fractal current sheet with many magnetic islands of different sizes connecting macroscopic and microscopic scales (Tajima and Shibata, 1997; Shibata, 1997, 1998; Tanuma *et al.*, 2001).

Let us first consider the Sweet-Parker current sheet with a thickness of δ_n and a length λ_n . This current sheet becomes unstable to secondary tearing if

$$t_n \leq \lambda_n / V_A, \quad (13)$$

where t_n is the growth time of the tearing instability at maximum rate ($\omega_{\max} \propto k_{\max}^{-2/5} t_{dif}^{-3/5} t_A^{-2/5}$ and $k_{\max} \propto (t_{dif}/t_A)^{-1/4}$, where ω_{\max} and k_{\max} are the maximum growth rate and corresponding wave number),

$$t_n \simeq (t_{dif} t_A)^{1/2} \simeq \left(\frac{\delta_n^2}{\eta V_A} \right)^{1/2}, \quad (14)$$

and λ_n/V_A is the time for the reconnection flow to carry the perturbation out of the current sheet. (As for the theory of the secondary tearing in the Sweet-Parker sheet, see e.g., Sonnerup and Sakai (1981), Biskamp (1992).) That is, if $t_n > \lambda_n/V_A$, the tearing instability is stabilized by the effect of flow. Using Eqs. (13) and (14), we find

$$\delta_n^3 \leq \eta V_A \left(\frac{\lambda_n}{V_A} \right)^2,$$

i.e.,

$$\delta_n \leq \eta^{1/3} V_A^{-1/3} \lambda_n^{2/3}. \quad (15)$$

If this inequality is satisfied, the secondary tearing occurs, leading to the current sheet thinning in the nonlinear stage of the tearing instability. At this stage, the current sheet thickness is determined by the most unstable wavelength of the secondary tearing instability, i.e.,

$$\begin{aligned} \lambda_{n+1} &\simeq 6\delta_n R_{m*,n}^{1/4} = 6\eta^{-1/4} V_A^{1/4} \delta_n^{5/4} \\ &\leq 6\eta^{1/6} V_A^{-1/6} \lambda_n^{5/6}, \end{aligned} \quad (16)$$

²This kind of evolution occurs when 1) the current sheet length is limited (Tanuma *et al.*, 2001), 2) magnetic field distribution is non-uniform around the current sheet (Magara *et al.*, 1997).

where $R_{m*,n} = \delta_n V_A / \eta$. The current sheet becomes thinner and thinner, and when the current sheet thickness becomes

$$\delta_{n+1} \leq \eta^{1/3} V_A^{-1/3} \lambda_{n+1}^{2/3}, \quad (17)$$

further secondary tearing occurs, and the same process occurs again at a smaller scale (Fig. 6). It follows from Eqs. (16) and (17) that

$$\delta_n \leq \left(\frac{\eta}{V_A} \right)^{1/6} 6^{2/3} \delta_{n-1}^{5/6}, \quad (18)$$

or

$$\frac{\delta_n}{L} \leq A \left(\frac{\delta_{n-1}}{L} \right)^{5/6}, \quad (19)$$

where

$$A = 6^{2/3} R_m^{-1/6}, \quad (20)$$

and

$$R_m = \frac{L V_A}{\eta}. \quad (21)$$

This fractal process continues until the current sheet thickness reaches the microscopic scale such as the ion Larmor radius or ion inertial length. The equation (19) leads to

$$\frac{\delta_n}{L} = A^{6(1-x)} \left(\frac{\delta_0}{L} \right)^x, \quad (22a)$$

where

$$x = (5/6)^n. \quad (22b)$$

From this, we can estimate how many secondary tearings are necessary for the initial macroscopic current sheet to reach the microscopic scale. Taking the typical solar coronal values, $\delta_0 = 10^8$ cm, $L = 10^9$ cm, $V_A = 10^8$ cm/s, $\eta = 10^4$ cm²/s for $T = 10^6$ K, we find $R_m = 10^{13}$ and

$$A \simeq 0.02. \quad (23)$$

Since δ_n must be smaller than the typical microscopic scale, e.g., the ion Larmor radius (~ 100 cm), we have

$$\delta_n / L < r_{L,ion} / L, \quad (24)$$

or

$$(0.02)^{6(1-(5/6)^n)} (0.1)^{(5/6)^n} < 10^{-7}.$$

The solution of this inequality (see Fig. 7) is

$$n \geq 6. \quad (25)$$

That is, in the solar corona, six secondary tearings are necessary to reach microscopic current sheet.

What is the time scale of this fractal tearing? The time scale for the n -th tearing is

$$t_n \simeq \delta_n^{3/2} (\eta V_A)^{-1/2} = (\delta_n / \delta_0)^{3/2} t_0, \quad (26)$$

where

$$t_0 = \delta_0^{3/2} / (\eta V_A)^{1/2}. \quad (27)$$

Since Eq. (22) leads to

$$\delta_n / \delta_0 \simeq A_0^{6(1-(5/6)^n)}, \quad (28)$$

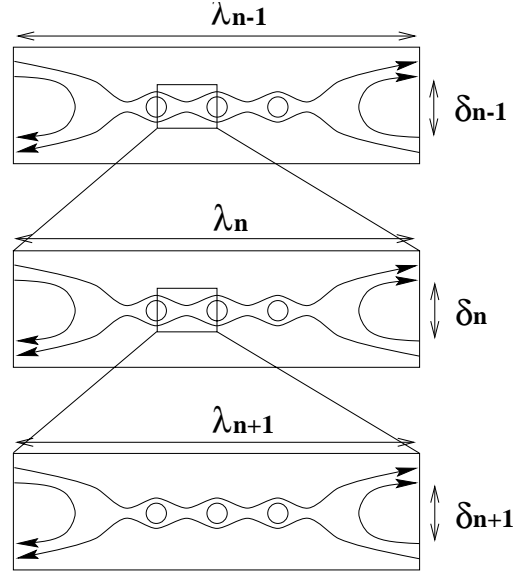


Fig. 6. Schematic view of fractal reconnection.

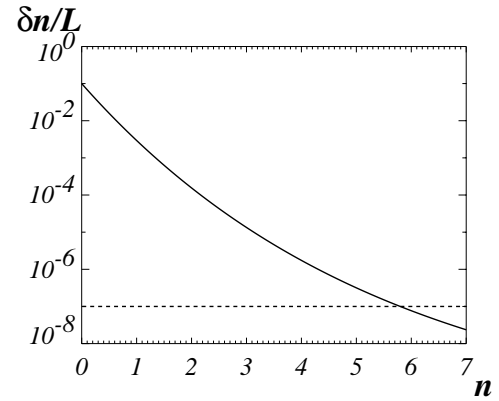


Fig. 7. The current sheet thickness (δ_n/L) in the n -th secondary tearing (see Eq. (22a)).

where $A_0 = 6^{2/3} R_{m*,0}^{-1/6}$, and $R_{m*,0} = \delta_0 V_A / \eta$, we find

$$t_n \simeq A_0^{9(1-(5/6)^n)} t_0. \quad (29)$$

Thus we obtain

$$t_n / t_{n-1} = A_0^{(3/2)(5/6)^{n-1}} \leq A_0^{3/2} \quad (30)$$

for $n \geq 1$. It follows from this equation that

$$t_n \leq A_0^{3/2} t_{n-1} \leq A_0^{(3/2)n} t_0. \quad (31)$$

Consequently, the total time from the 1st (secondary) tearing (t_1) to the n -th (secondary) tearing (t_n) becomes

$$t_{total} = t_1 + t_2 + \dots + t_n \leq t_0 A_0^{3/2} \frac{1 - A_0^{3n/2}}{1 - A_0^{3/2}} \leq t_0 A_0^{3/2}. \quad (32)$$

For typical coronal conditions (described above), this time scale becomes

$$t_{total} \leq 6 \times 10^{-3} t_0, \quad (33)$$

which is much shorter than the time scale of the 0-th tearing (t_0). Although the 0-th tearing time is long ($\sim 3 \times 10^4 - 10^6$ sec for initial current sheet with $\delta_0 \sim 10^7 - 10^8$ cm), the nonlinear fractal tearing time is quite short (less than $10^2 - 3 \times 10^3$ sec), so that the microscopic scale is easily reached within a short time as a result of the fractal tearing.

It should be stressed that the role of the fractal tearing is only to produce a very thin current sheet with a microscopic scale of order of the ion Larmor radius or the ion inertial length. The fractal tearing does not explain the main energy release in flares. The main energy release is explained by the fast reconnection process which occurs after the ejection of the large scale plasmoid as we discussed before.

6. Summary: A Scenario for Fast Reconnection

Let us summarize our scenario of fast reconnection in the solar corona, which is illustrated in Figs. 8 and 9 (the latter is from a numerical simulation by Tanuma *et al.*, 2001 and it nicely illustrates a part of our scenario). Our scenario can also be applied to other hot astrophysical plasmas (e.g., stellar corona, interstellar medium, galactic halo, galactic clusters, and so on) for which magnetic Reynolds number and the ratio of its characteristic scale length to the ion Larmor radius (or ion inertial length) are very large.

Initially we assume the current sheet whose thickness is much larger than the microscopic plasma scale. Such a current sheet is easily created by the interaction of emerging flux with an overlying coronal field (e.g., Heyvaerts *et al.*, 1977; Shibata *et al.*, 1992; Yokoyama and Shibata, 1995), the collision of a moving bipole with other magnetic structure (e.g., Priest *et al.*, 1994), the global resistive MHD instability in a shearing arcade (e.g., Mikic *et al.*, 1988; Biskamp and Welter, 1989; Kusano *et al.*, 1995; Choe and Lee, 1996; Magara *et al.*, 1997; Choe and Cheng, 2000; Cheng and Choe, 2001), or other related mechanisms (e.g., Forbes, 1990; Chen *et al.*, 2001).

If the current sheet length becomes longer than the critical wavelength for the tearing mode instability, the instability starts. As the instability develops, it enters a nonlinear regime which makes the initial current sheet thinner and thinner. The current sheet thinning stops when the sheet thickness becomes comparable to that of the Sweet-Parker sheet, and thereafter the sheet length increases with time. If the sheet length becomes longer than a critical wavelength (Eq. (13)), secondary tearing occurs. Even if the sheet has not yet reached the Sweet-Parker state, it can become unstable to the secondary tearing if the sheet thickness satisfies the same condition (Eq. (13)). Then the same process occurs again at a smaller scale, and the system evolves into one that is fractally structured. In this way, a microscopically small scale (such as ion Larmor radius or ion inertial length) can be reached within a short time.

Once a small scale is achieved, fast reconnection occurs because anomalous resistivity can now set in. It is also possible that fast collisionless reconnection occurs with a nondimensional reconnection rate of the order of 0.1–0.01 at this small scale (see recent full particle simulations by, e.g., Drake, 2000; Hoshino *et al.*, 2001; Tanaka, 2001; Horiuchi *et al.*, 2001). Hence small scale magnetic islands (plasmoids) created by small scale tearing are ejected at the Alfvén

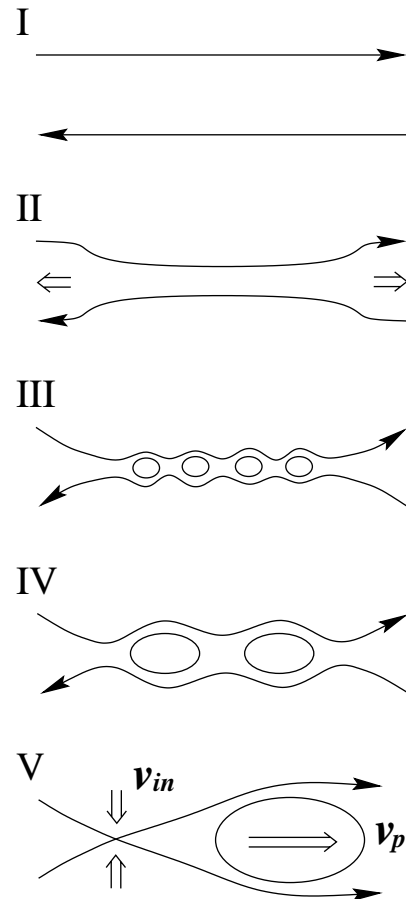


Fig. 8. A scenario for fast reconnection. I: The initial current sheet. II: The current sheet thinning in the nonlinear stage of the tearing instability or global resistive MHD instability. The current sheet thinning stops when the sheet evolves to the Sweet-Parker sheet. III: The secondary tearing in the Sweet-Parker sheet. The current sheet becomes fractal because of further secondary tearing as shown in Fig. 6. IV: The magnetic islands coalesce with each other to form bigger magnetic islands. The coalescence itself proceeds with a fractal nature. In the phases III and IV, the microscopic plasma scale (ion Larmor radius or ion inertial length) is reached, so that fast reconnection becomes possible at small scales, V: The greatest energy release occurs when the largest plasmoid (magnetic island or flux rope) is ejected. The maximum inflow speed (V_{in} = reconnection rate) is determined by the velocity of the plasmoid (V_p). Hence this reconnection is called *plasmoid-induced-reconnection*.

speed and collide with other islands to coalesce with each other, thereby making bigger islands (plasmoids). This coalescing process itself also occurs with a fractal nature (Tajima and Shibata, 1997).

It should be noted that the ejection (acceleration) of plasmoids (flux rope with axial field in 3D space) can enhance the inflow into the reconnection point, creating a positive feedback, i.e., nonlinear instability (as we outlined in Section 4). This determines the macroscopic reconnection rate which may be smaller or larger than the microscopic reconnection rate. If the macroscopic reconnection rate (inflow speed) is larger than the microscopic reconnection rate, the magnetic flux is accumulated around the diffusion region, leading to intermittent fast reconnection (Lee and Fu, 1986; Kitabata *et al.*, 1996; Schumacher and Kliem, 1996; Tanuma *et al.*, 1999, 2001; Fig. 9). On the other hand, if the macroscopic reconnection rate is smaller than the mi-

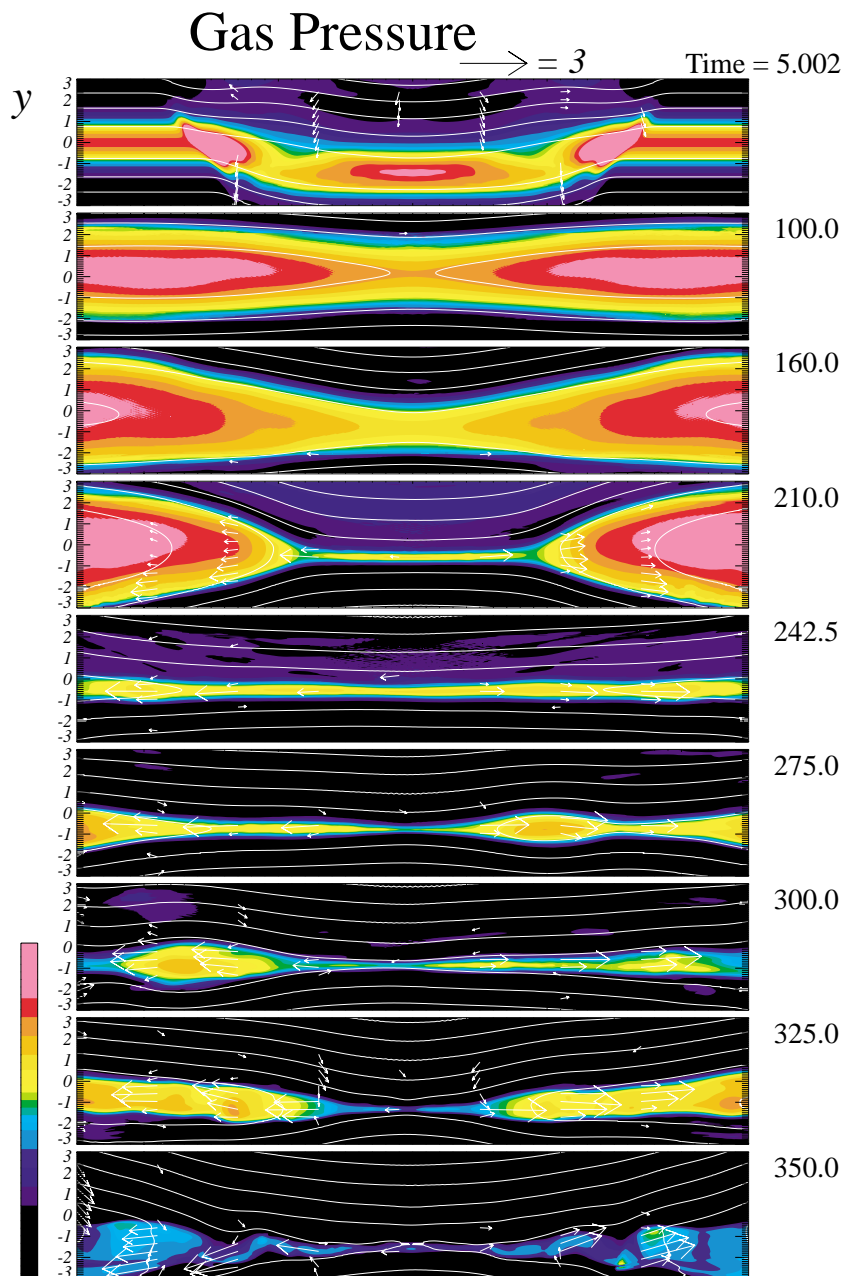


Fig. 9. Numerical simulation of reconnection triggered by an MHD fast mode shock (Tanuma *et al.*, 2001), illustrating a part of our proposed scenario for fast reconnection (Fig. 8): a) passage of the MHD fast shock, b) current sheet thinning (in the nonlinear stage of the tearing instability), c) the Sweet-Parker reconnection, d) secondary tearing, e) Petschek reconnection as a result of the onset of anomalous resistivity. Slow shocks inherent to Petschek reconnection are formed.

crossopic reconnection rate, the reconnection may continue in a quasi-steady state. However, there may be large amplitude perturbations around the reconnection point, so that it would be difficult to maintain quasi-steady reconnection. The reconnection would be very time dependent with intermittent reconnection and ejection of plasmoids with various sizes created by fractal reconnection. Petschek's slow shocks are also formed in a very time dependent manner (e.g., Yokoyama and Shibata, 1994; Tanuma *et al.*, 2001). The local macroscopic reconnection rate can be much larger than the average reconnection rate and is determined by the macroscale dynamics, i.e., *plasmoid-induced-reconnection*.

In this case, the time dependence is essential for determining the reconnection rate.

Since this process is scale free, we have fractal structure in the global current sheet. The greatest energy release occurs when the largest plasmoid is ejected. This may correspond to the impulsive phase of flares. The time variation of the reconnection rate (and the total energy release rate) associated with ejection of plasmoids with various sizes is also fractal. That is, the power spectrum of the time variation of the reconnection rate and the energy release rate show a power-law distribution. This may correspond to the fragmented light curves of solar X-ray and radio emissions in

the impulsive phase of flares (e.g., Benz and Aschwanden, 1992).

Quantitative proof of the fractal nature of the current sheet (especially in 3D geometry) remains as an important subject for future numerical simulations and laboratory experiments, both of which will have to be able to handle much larger magnetic Reynolds number than they currently do (i.e., $R_m \simeq 10^3\text{--}10^4$) in order to solve this fundamental problem.

Acknowledgments. The authors would like to thank K. Dere, J. Drake, M. Hoshino, T. Magara, T. Morimoto, M. Ohya, Y. Ono, E. N. Parker, M. Scholer, M. Tanaka, T. Terasawa, M. Ugai, M. Yamada, and T. Yokoyama for fruitful discussions. They also thank T. Forbes and C. Z. Cheng for their careful reading of our manuscript and their many useful comments and suggestions which are very useful to improve the paper. Numerical computations were carried out on VPP300/16R and(or) VX/4R at the Astronomical Data Analysis Center of the National Astronomical Observatory, Japan, which is an inter-university research institute of astronomy operated by Ministry of Education, Science, Culture, and Sports.

Appendix. Derivation of Eqs. (6) and (10)

As we wrote in the text, we assume that all the mass convected into the reconnection region ($\rho V_i L_i$ per unit time per unit length in 2D space) are accelerated to Alfvén speed V_A . Since such accelerated mass (reconnection jet) collides with the plasmoid, it can accelerate the plasmoid. Denoting V_p = plasmoid speed, M_p = plasmoid mass, ΔM_p = mass convected by the reconnection jet during a short time Δt , which is equal to increase in plasmoid mass during Δt , we obtain the conservation of momentum as

$$\Delta M_p V_A + M_p V_p = (M_p + \Delta M_p)(V_p + \Delta V_p). \quad (\text{A.1})$$

Here the left hand side is the total momentum before collision, and the right hand side is the total momentum after collision. If we neglect the term ΔM_p in the right hand side of Eq. (A.1) (i.e., if we assume $V_p \ll V_A$), we have

$$M_p \Delta V_p = \Delta M_p V_A. \quad (\text{A.2})$$

The plasmoid mass (M_p) and the mass added to the plasmoid (ΔM_p) by the jet for a short time Δt are written as

$$M_p = \rho_p L_p W_p, \quad (\text{A.3})$$

$$\Delta M_p = \rho V_i L_i \Delta t, \quad (\text{A.4})$$

both of which are per unit length. Using these formulae, the equation (A.2) becomes $\rho_p L_p W_p \Delta V_p = \rho V_i L_i V_A \Delta t$, which is equivalent to

$$\rho_p L_p W_p \frac{dV_p}{dt} = \rho V_i L_i V_A. \quad (\text{A.5})$$

Since we assumed that the mass injection into reconnection region is induced by the plasmoid motion, i.e., $V_i L_i = V_p W_p$ (Eq. (5)), the right hand side of equation (A.5) becomes equal to $\rho V_p W_p V_A$, so that we get Eq. (6):

$$\rho_p L_p W_p \frac{dV_p}{dt} = \rho V_i L_i V_A = \rho V_p W_p V_A. \quad (6)$$

Note that in deriving above formulae, we did not assume conservation of kinetic energy. This is because some part of

the kinetic energy is dissipated to heat the plasmoid, leading to increase in gas pressure (internal energy) of the plasmoid. Although such enhanced gas pressure may accelerate the plasmoid further, we neglected the effect of gas pressure in above treatment for simplicity, since it is not easy to estimate how much fraction of internal energy is converted to the kinetic energy of a plasmoid.

When V_p grows to the value that cannot be neglected compared with V_A , we cannot neglect the term $\Delta M_p V_p$ in the right hand side of Eq. (A.1). In this case, the momentum conservation equation becomes $M_p \Delta V_p = (V_A - V_p) \Delta M_p$. Combining this equation with Eqs. (A.3) and (A.4), we get

$$\frac{dV_p}{dt} = \frac{\rho V_p}{\rho_p L_p} (V_A - V_p). \quad (\text{A.6})$$

If ρ , ρ_p , V_A , and L_p are constant in time, the solution of this equation becomes Eq. (10):

$$V_p = \frac{V_A \exp(\omega t)}{\exp(\omega t) - 1 + V_A/V_0}. \quad (10)$$

Here V_0 is the initial velocity of a plasmoid at $t = 0$, and $\omega = (\rho/\rho_p)(V_A/L_p)$.

References

- Akiyama, S. and H. Hara, X-ray eruptive structures associated with small flares, *Adv. Space Res.*, **26**, 465–468, 2000.
- Anzer, U. and G. W. Pneuman, Magnetic reconnection and coronal transients, *Solar Phys.*, **79**, 129–147, 1982.
- Benz, A. O. and M. J. Aschwanden, Characteristics of the impulsive phase of flares, in *Proc. Eruptive Solar Flares, IAU Colloq. No. 133*, edited by Z. Svestka, B. V. Jackson, and M. E. Machado, Lecture Notes in Physics 399, Springer-Verlag, Berlin, pp. 106–115, 1992.
- Biskamp, D., Magnetic reconnection via current sheets, *Phys. Fluids*, **29**, 1520–1531, 1986.
- Biskamp, D., Nonlinear Magnetohydrodynamics, 392 pp., Cambridge Univ. Press, 1992.
- Biskamp, D. and H. Welter, Magnetic arcade evolution and instability, *Solar Phys.*, **120**, 49–77, 1989.
- Carmichael, H., A process for flares, in *Proc. AAS-NASA Symp. on the Physics of Solar Flares*, edited by W. N. Hess, Washington, NASA, NASA-SP 50, pp. 451–456, 1964.
- Chen, P. F., K. Shibata, and T. Yokoyama, Global destabilization due to localized reconnection: a mechanism for coronal mass ejections, *Earth Planets Space*, **53**, this issue, 611–614, 2001.
- Cheng, C. Z. and G. S. Choe, Solar flare mechanism based on magnetic arcade reconnection and island merging, *Earth Planets Space*, **53**, this issue, 597–604, 2001.
- Choe, G. S. and L. Lee, Evolution of solar magnetic arcades. I. Ideal MHD evolution under footpoint shearing, *ApJ*, **472**, 360–371, 1996.
- Choe, G. S. and C. Z. Cheng, A model of solar flares and their homologous behavior, *ApJ*, **541**, 449–467, 2000.
- Dere, K., G. E. Brueckner, R. A. Howard, D. J. Michels, and J. P. DeLaboudiniere, LASCO and EIT observations of helical structure in coronal mass ejections, *ApJ*, **516**, 465–474, 1999.
- Drake, J., private communication, 2000.
- Forbes, T. G., Numerical simulation of a catastrophe model for coronal mass ejections, *J. Geophys. Res.*, **95**, 11919–11931, 1990.
- Forbes, T. G. and L. Acton, Reconnection and field line shrinkage in solar flares, *ApJ*, **459**, 330–341, 1996.
- Hanaoka, Y., H. Kurokawa, S. Enome *et al.*, Simultaneous observations of a prominence eruption followed by a coronal arcade formation in radio, soft X-rays, and H alpha, *PASJ*, **46**, 205–216, 1994.
- Heyvaerts, J., E. R. Priest, and D. Rust, An emerging flux model for the solar flare phenomenon, *ApJ*, **216**, 123–137, 1977.
- Hirayama, T., Theoretical model of flares and prominences. I. Evaporating flare model, *Solar Phys.*, **34**, 323–338, 1974.
- Hirayama, T., Magnetic morphologies of solar flares, in *Lecture Note in Physics, No. 387, Flare Physics in Solar Activity Maximum 22*, edited by Y. Uchida *et al.*, pp. 197–201, Springer, New York, 1991.

- Horiuchi, R., W. Pei, and T. Sato, Collisionless driven reconnection in an open system, *Earth Planets Space*, **53**, this issue, 439–445, 2001.
- Hoshino, M., K. Hiraide, and T. Mukai, Strong electron heating and non-Maxwellian behavior in magnetic reconnection, *Earth Planets Space*, **53**, this issue, 627–634, 2001.
- Hundhausen, A., Coronal mass ejections, in *The Many Faces of the Sun: A Summary of the Results from NASA's Solar Maximum Mission*, edited by K. T. Strong, J. L. R. Saba, B. M. Haisch, and J. T. Schmelz, pp. 143–200, Springer, New York, 1999.
- Ichimaru, S., Electrical resistivity of electromagnetically turbulent plasma and reconnection rate of magnetic fields, *ApJ*, **202**, 524–531, 1975.
- Kahler, S. W., R. L. Moore, S. R. Kane, and H. Zirin, Filament eruptions and the impulsive phase of solar flares, *ApJ*, **328**, 824–829, 1988.
- Kitabata, H., T. Hayashi, T. Sato *et al.*, Impulsive nature in magnetohydrodynamic driven reconnection, *J. Phys. Soc. Japan*, **65**, 3208–3214, 1996.
- Kopp, R. A. and G. W. Pneuman, Magnetic reconnection in the corona and the loop prominence phenomenon, *Solar Phys.*, **50**, 85–98, 1976.
- Kusano, K., Y. Suzuki, and K. Nishikawa, A solar flare triggering mechanism based on the Woltjer-Taylor minimum energy principle, *ApJ*, **441**, 942–951, 1995.
- Lee, L. C. and Z. F. Fu, Multiple X line reconnection, I. A criterion for the transition from a single X line to a multiple X line reconnection, *J. Geophys. Res.*, **91**, 6807–6815, 1986.
- Lin, J. and T. G. Forbes, Effects of reconnection on the coronal mass ejection process, *J. Geophys. Res.*, **105**, 2375–2392, 2000.
- Magara, T., K. Shibata, and T. Yokoyama, Evolution of eruptive flares. I. Plasmoid dynamics in eruptive flares, *ApJ*, **487**, 437–446, 1997.
- Magara, T. and K. Shibata, Evolution of eruptive flares. II. The occurrence of locally enhanced resistivity, *ApJ*, **514**, 456–471, 1999.
- Masuda, S., T. Kosugi, H. Hara, S. Tsuneta, and Y. Ogawara, A loop-top hard X-ray source in a compact solar flare as evidence for magnetic reconnection, *Nature*, **371**, 495–496, 1994.
- Mikic, Z., D. C. Barnes, and D. D. Schnack, Dynamical evolution of a solar coronal magnetic field arcade, *ApJ*, **328**, 830–847, 1988.
- Moore, R. L. and G. Roumeliotis, Triggering of eruptive flares: destabilization of the preflare magnetic field configuration, in *Lecture Note in Physics, No. 399, Eruptive Flares*, edited by Z. Svestka, B. V. Jackson, and M. E. Machado, pp. 69–78, Springer, New York, 1992.
- Morimoto, T. and H. Kurokawa, private communication, 2000.
- Nitta, S., S. Tanuma, K. Maezawa, and K. Shibata, Fast magnetic reconnection in free space: self-similar evolution process, *ApJ*, **550**, 1119–1130, 2001.
- Nitta, N., A study of major solar flares observed by Yohkoh, in *Magnetic Reconnection in the Solar Atmosphere*, ASP Conference Series; Vol. 111, edited by R. D. Bentley and J. T. Mariska (1997), pp. 156–161, 1996.
- Ohyama, M. and K. Shibata, Preflare heating and mass motion in a solar flare associated with hot plasma ejection: 1993 November 11 C9.7 flare, *PASJ*, **49**, 249–261, 1997.
- Ohyama, M. and K. Shibata, X-ray plasma ejection associated with an impulsive flare on 1992 October 5: physical conditions of X-ray plasma ejection, *ApJ*, **499**, 934–944, 1998.
- Ohyama, M. and K. Shibata, Timing and occurrence rate of X-ray plasma ejections, *JASTP*, **62**, 1509–1514, 2000.
- Ono, Y., M. Inomoto, Y. Ueda, T. Matsuyama, and Y. Murata, Fast compression of a current sheet during externally driven magnetic reconnection, *Earth Planets Space*, **53**, this issue, 521–526, 2001.
- Priest, E. R., C. E. Parnel, and S. F. Martin, A converging flux model of an X-ray bright point and an associated canceling magnetic feature, *ApJ*, **427**, 459–474, 1994.
- Scholer, M., Undriven magnetic reconnection in an isolated current sheet, *J. Geophys. Res.*, **94**, 8805–8812, 1989.
- Schumacher, J. and B. Kliem, Dynamic current sheets with localized anomalous resistivity, *Phys. Plasmas*, **3**, 4703–4711, 1996.
- Shibata, K., S. Nozawa, and R. Matsumoto, Magnetic reconnection associated with emerging magnetic flux, *PASJ*, **44**, 265–271, 1992.
- Shibata, K., S. Masuda, M. Shimojo, H. Hara *et al.*, Hot plasma ejections associated with compact-loop solar flares, *Ap. J. Lett.*, **451**, L83–L85, 1995.
- Shibata, K., New observational facts about solar flares from Yohkoh studies—Evidence of magnetic reconnection and a unified model of flares, *Adv. Space Res.*, **17**, (4/5)9–18, 1996.
- Shibata, K., Rapidly time variable phenomena: Jets, explosive events, and flares, 1997, in Proc. 5-th SOHO workshop, ESA, SP-404, pp. 103–112, 1997.
- Shibata, K., A unified model of flares, in *Proc. Observational Plasma Astrophysics: Five Years of Yohkoh and Beyond*, edited by T. Watanabe *et al.*, pp. 187–196, 1998.
- Shibata, K., Evidence of magnetic reconnection in solar flares and a unified model of flares, *Astrophys. Sp. Sci.*, **264**, 129–144, 1999.
- Simnett, G. M., S. J. Tappin, S. P. Plunkett, D. K. Beaford *et al.*, LASCO observations of disconnected magnetic structures out to beyond 28 solar radii during coronal mass ejections, *Solar Phys.*, **175**, 685–698, 1997.
- Sonnerup, B. U. O. and J.-I. Sakai, Stability of a current sheet with resistive MHD stagnation point flows, *EOS Trans. Amer. Geophys. Union*, **62**, 353 (abstract), 1981.
- Sturrock, P. A., Model of the high energy phase of solar flares, *Nature*, **211**, 695–697, 1966.
- Tajima, T. and K. Shibata, *Plasma Astrophysics*, p. 494, Addison-Wesley, Reading, 1997.
- Tanaka, M., The origins of electrical resistivity in magnetic reconnection: Studies by 2D and 3D macro particle simulations, *Earth Planets Space*, **53**, this issue, 463–472, 2001.
- Tanuma, S., T. Yokoyama, T. Kudoh, R. Matsumoto, K. Shibata, and K. Makishima, Magnetic reconnection as the origin of galactic-ridge X-ray emission, *PASJ*, **51**, 161–172, 1999.
- Tanuma, S., T. Yokoyama, T. Kudoh, and K. Shibata, Two-dimensional MHD numerical simulations of magnetic reconnection triggered by a supernova shock in interstellar medium: generation of X-ray gas in galaxy, *ApJ*, **551**, 312–332, 2001.
- Treumann, R. A. and W. Baumjohann, *Advanced Space Plasma Physics*, 381 pp., Imperial College, London, 1997.
- Tsuneta, S., H. Hara, T. Shimizu, L. Acton *et al.*, Observation of a solar flare at the limb with the YOHKOH soft X-ray telescope, *PASJ*, **44**, L63–L69, 1992a.
- Tsuneta, S., T. Takahashi, L. Acton, M. Bruner *et al.*, Global restructuring of the coronal magnetic fields observed with the YOHKOH soft X-ray telescope, *PASJ*, **44**, L211–214, 1992b.
- Tsuneta, S., Moving plasmoid and formation of the neutral sheet in a solar flare, *ApJ*, **483**, 507–514, 1997.
- Ugai, M., Spontaneously developing magnetic reconnections in a current-sheet system under different sets of boundary conditions, *Phys. Fluids*, **25**, 1027–1037, 1982.
- Ugai, M., Global dynamics and rapid collapse of an isolated current-sheet system enclosed by free boundaries, *Phys. Fluids*, **29**, 3659–3667, 1986.
- Ugai, M., Computer studies on development of the fast reconnection mechanism for different resistivity models, *Phys. Fluids B*, **4**, 2953–2963, 1992.
- Yan, M., L. Lee, and E. R. Priest, Fast magnetic reconnection with small shock angles, *J. Geophys. Res.*, **98**, 8277–8293, 1992.
- Yokoyama, T. and K. Shibata, What is the condition for fast magnetic reconnection?, *ApJ*, **436**, L197–L200, 1994.
- Yokoyama, T. and K. Shibata, Magnetic reconnection as the origin of X-ray jets and H-alpha surges on the Sun, *Nature*, **375**, 42–44, 1995.
- Yokoyama, T. and K. Shibata, Magnetohydrodynamic simulation of a solar flare with chromospheric evaporation effect based on magnetic reconnection model, *ApJ*, **549**, 1160–1174, 2001.